MAPPING CRATERS DEPTHS IN TERRA CIMMERIA, MARS: IMPLICATIONS FOR SPATIAL DISTRIBUTION OF GROUND ICE. Tomasz. F. Stepinski[1] and Erik R. Urbach[1], [1]Lunar and Planetary Institute, 3600 Bay Area Blvd., Houston, TX 77058, USA. (tom@lpi.usra.edu, Urbach@lpi.usra.edu).

Introduction: It is widely believed that a significant quantity of water resides in Martian subsurface in the form of ground ice. Thermodynamic models have been used [1,2,3] to calculate an extent of the cryosphere, a zone in the subsurface where ground ice is stable. The models predict that both, the depth of the upper boundary (z_0) of the cryosphere and the depth of its lower boundary (z_1) are functions of latitude In particular, $z_0 \approx 0$ at high latitudes, but is lowered by a few hundred meters at the equatorial zone [1,2,3]. As the ground ice is not directly observable (a situation that may be changing with deployment of ground penetrating radar instruments), we have to rely on surface expressions of ground ice for model verification. Morphology of impact craters is often used to infer presence of ground ice. Spatial distribution of rampart craters shows [4,5] that their onset diameter decreases polewards from the equator in agreement with decreasing value of z_0 as predicted by the cryosphere models. Similarly, softened terrain, a style of crater degradation attributed to viscous relaxation of topography on icy crust, is found only at higher latitudes [6].

This evidence was obtained on the basis of subjective, visual inspection of imagery data. In [7] it was demonstrated that visual differences between softened and unsoftened craters can be quantified by measuring several crater parameters. Thus, mapping spatial variability of craters parameters constitutes a plausible method for objective determination of spatial distribution of ground ice. However, manual measurement of such parameters for a sufficiently large number of craters to cover an area of interest is too labor intensive and thus impractical. Recently we have developed [8,9] a robust crater detection algorithm (CDA) capable of identifying and characterizing virtually all craters in a given site having diameter $D \geq 3$ km. We have applied this CDA to the Terra Cimmeria region on Mars located between 120°E – 180°E and 0°S – 90°S and dominated by Noachian age surfaces. The algorithm identifies craters and calculates their diameters (D) and depths (d). These data is used to construct raster maps of depth-to-diameter ratio (d/D) for craters in different size bins. The maps are used to infer spatial distribution and properties of ground ice.

Methods: Our CDA is a two stage system that uses topography data as given by the MOLA Mission Experiment Gridded Data Record (MEGDR) [10] with resolution of 1/128 degree. The details of the CDA are given in [8,9]. Reliance on topographic data instead of imagery, used in previous attempts to automate crater detection, gives our CDA a necessary robustness, but it also restricts the size of craters that can be detected. Applying the CDA to the Terra Cimmeria region results in a catalog of 7845 craters listing their positions and the values of D and d.

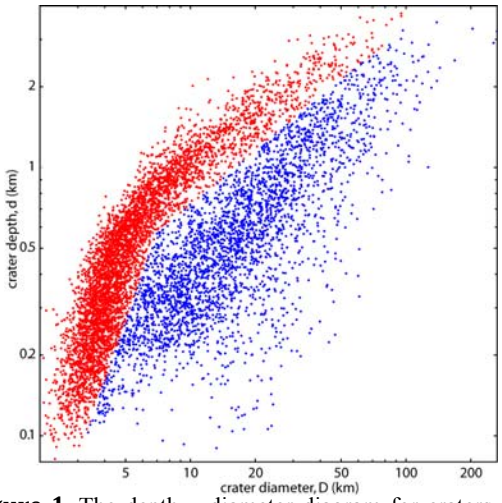

Figure 1. The depth – diameter diagram for craters in the Terra Cimmeria region. The red indicate "deep" craters and the blue indicate "shallow craters."

Fig.1 shows the depth-diameter diagram constructed on the basis of this catalog. The current version of our CDA does not assign any morphologic labels to the craters, thus the catalog carries no information on whether the craters are fresh or degraded, rampart or not, softened or unsoftened. However, inspection of Fig.1 reveals the existence of two populations of craters which we refer to as "deep" and "shallow." The deep craters follow the broken power law relation between D and d with the brake separating simple from complex craters occurring at $D_* \approx 7$ km.

Identified craters are divided into six size bins, $D < 5$ km , $5 \text{ km} \leq D < 10$ km, $10 \text{ km} \leq D < 15$ km, $15 \text{ km} \leq D < 20$ km, $20 \text{ km} \leq D < 25$km, $D \geq 25$ km. Using craters from each bin separately a raster map with resolution of 0.5 degree is constructed to show spatial variation of d/D. The value of d/D at each pixel of the map is calculated as an average of the values of d/D for individual craters located within a 2 degree square window centered at that pixel. In cases where there are no craters within a window a "nodata" entry is assigned to a pixel.

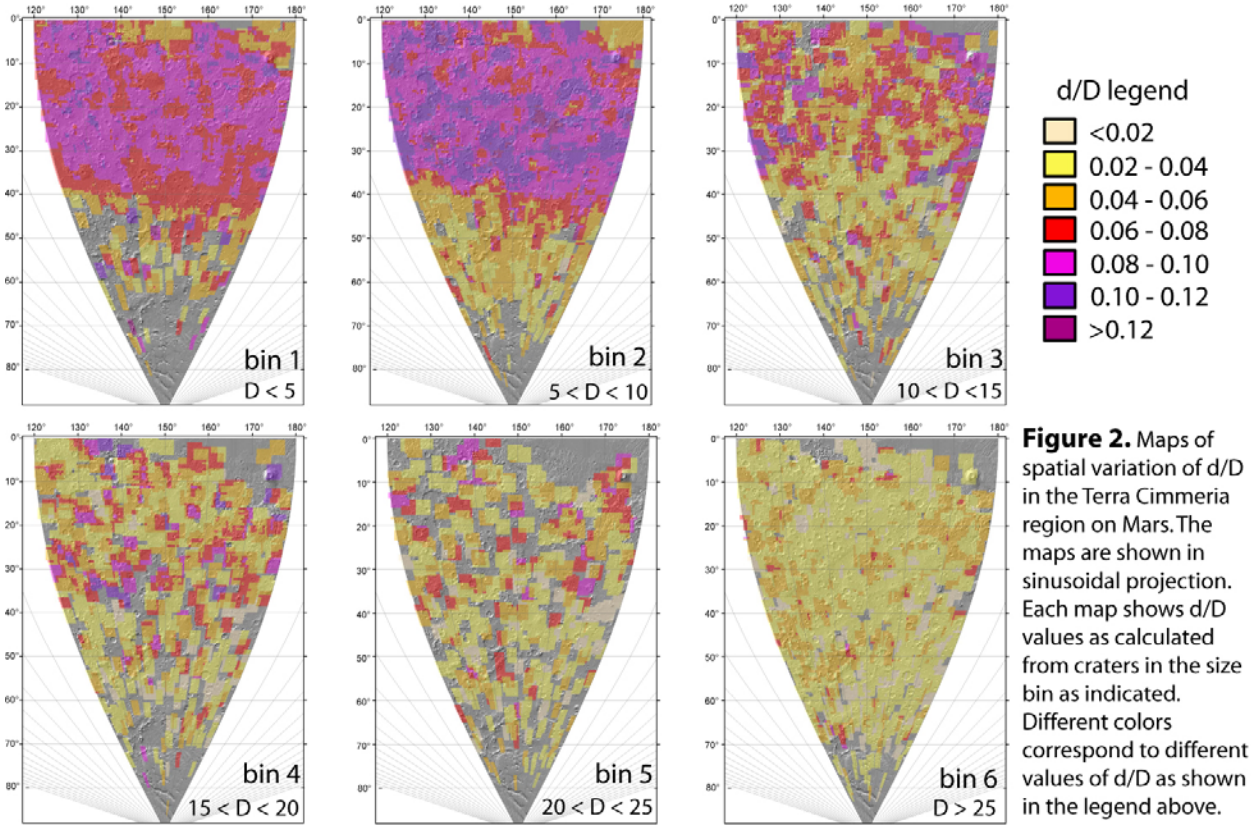

Figure 2. Maps of spatial variation of d/D in the Terra Cimmeria region on Mars. The maps are shown in sinusoidal projection. Each map shows d/D values as calculated from craters in the size bin as indicated. Different colors correspond to different values of d/D as shown in the legend above.

Results: Fig.2 shows the raster maps of d/D for all six crater size bins. The red-to-purple colors indicate high values of d/D, and the yellow-to-orange colors indicate low values of d/D. The maps reveal existence of three different regimes of spatial patterns. (1) For craters with D < 10 km (the first two size bins) there is a clear binary pattern. The Terra Cimmeria region is divided into two zones, the "equatorial" zone ($Zone_E$) extending from the equator to the latitude of ~ 40°S, and the "high latitude" zone ($Zone_{HL}$) extending from to the latitude of ~ 40°S to the south pole. In $Zone_E$ the craters are deep, the average value of d/D is ~ 0.09, whereas in $Zone_{HL}$ the craters are shallow, the average value of d/D is ~ 0.049. (2) For craters with D > 25 km (the sixth size bin) there is no spatial pattern, the entire Terra Cimmeria region is characterized by the same range of d/D values. The average value of d/D is ~ 0.033. (3) For craters with 10 km < D < 25 km (the third to fifth size bins) the binary pattern, so pronounced for craters in the smaller size bins, is progressively weaker. The $Zone_{HL}$ has the same character as in the smaller size bins; the craters are shallow, average value of d/D changes from ~ 0.04 in the third bin to ~ 0.034 in the fifth bin. However, the $Zone_E$ has a no-uniform, patchy character, a mixture of location where craters are deep with location where they are shallow. With increasing value of D the number of patches with deep craters decreases. Average value of d/D changes from ~ 0.06 in the third bin to ~ 0.046 in the fifth bin.

Fig.3 shows the crater data, divided into the same size bins, displayed as a series of (d/D)-latitude diagrams. It offers an additional insight into distribution of craters in the Terra Cimmeria region. Deep and shallow populations of craters, as defined on Fig.1, are displayed in different colors. Examination of Fig.3 confirms observations made on the basis of studying Fig.2. $Zone_E$ and $Zone_{HL}$, identified on the basis of maps in Fig.2, are also seen on diagrams in Fig.3. There is a strong d/D dichotomy between the two zones with respect to the craters in the first two size bins. This dichotomy gradually disintegrates when craters in progressively larger size bins are examined. Finally, no $Zone_E$/$Zone_{HL}$ dichotomy is observed with respect to the craters in the largest size bin. Because all individual craters are shown on Fig.3, one can also get a sense of how the crater density changes with latitude. In particular, a severe depletion of smallest craters in the $Zone_{HL}$ is clearly visible.

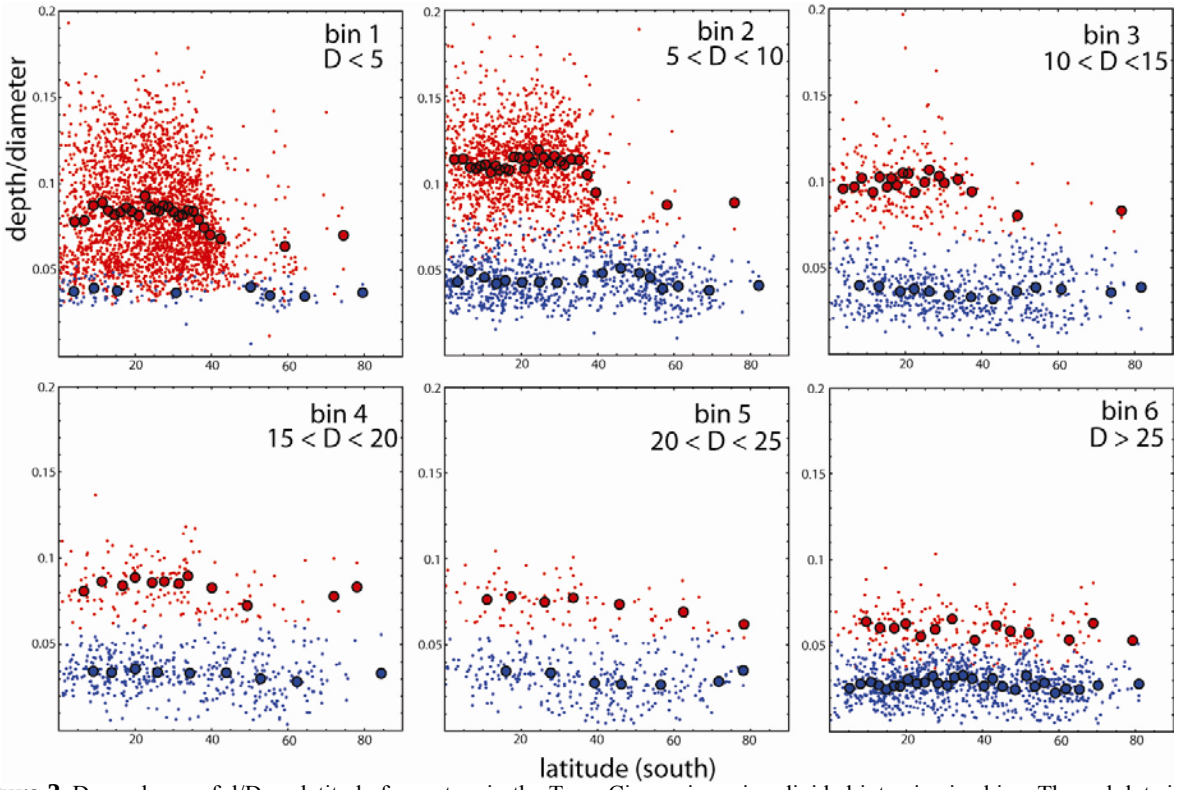

Figure 3. Dependence of d/D on latitude for craters in the Terra Cimmeria region divided into six size bins. The red dots indicate "deep" craters and blue indicate "shallow craters" as defined on Fig.1. Circles indicate trends calculated by binning the data. The horizontal distance between circles is a measure of density of craters. Different binning is performed on each crater category.

Discussion: The patterns on Figs.2 and 3 support the results of [4,5, and 7]; most craters located at high latitudes have different shapes than craters located closer to the equator. Although individual features of patterns seen on Figs.2 and 3 could be conceivably explained by a number of mechanisms, the entire set of observed patterns is best explained by an existence of the cryosphere with z_0 significantly lowered in the equatorial regions, just as predicted by models based on ice stability concept. Moreover, our results extend the past evidence supporting such models. We have established 40°S as the latitude where upper boundary of cryosphere transits from substantial depth in *Zone*$_E$ to near surface at *Zone*$_{HL}$. In addition, a patchy disintegration of the "deep" character of *Zone*$_E$ with increasing crater size (see size bins 3 to 5 on Fig.2) suggests depth variability of the upper boundary of the cryosphere .

Our results are amenable to quantitative analysis, given a set of assumptions about impact cratering process, crater degradation process, as well as the structure of the subsurface itself. In the following analysis we assume an idealized scenario wherein initial crater shapes are independent of surface material properties and the viscous relaxation due to presence of ground ice is the only crater modification process. Furthermore, our estimates are based on calculations [11,12,13] which are subject to additional simplifications.

Both, analytic [11] and numerical [12,13] calculations have been carried out to asses the changes to crater shape due to viscous relaxation. The upshot of the calculations is that the style of crater modification depends on the z_1/D ratio. For $z_1/D > (z_1/D)_*$, corresponding to a crater placed in a cryosphere that is deep relative to the crater size, the dominant modification effect is raising of the crater floor resulting in significant decrease of crater's d/D value. For $z_1/D < (z_1/D)_*$, corresponding to a crater placed in a cryosphere that is shallow relative to the crater size, the dominant modification effect is rounding off and some dropping of the crater rim resulting in a small to moderate decrease of crater's d/D value. The threshold value is $(z_1/D)_* \sim 1/(2\pi) \approx 0.16$.

Spatial patterns seen on the maps of d/D featured in Fig.2 are consistent with the viscous relaxation model,

and provide numerical constrains on the shape and the character the cryosphere. First, the dichotomy pattern observed for craters with D < 10 km constrains the location of z_0. In *Zone*$_E$ the high values of d/D indicate absence of viscous relaxation. Thus z_0 must be located deeper than the depth of 10-km-size craters located in the *Zone*$_E$, or $z_0 \geq 0.9$ km. In *Zone*$_{HL}$ there is a striking absence of the smallest craters (the first bin). According to numerical modeling [13] a relaxation time scale for craters of that size may be short enough to erase their topographic expression explaining their absence in our catalog. The slightly bigger craters in *Zone*$_{HL}$ (the second bin) are characterized by low values of d/D indicating presence of viscous relaxation in the $z_1/D > (z_1/D)_*$ regime and thus $z_0 \approx 0$. The *Zone*$_E$/*Zone*$_{HL}$ boundary is centered at 40°S, but it does not strictly follow single latitude.

Second, the lack of spatial variability in d/D for craters with D ≥ 25 km constrains the location of z_1. The similarity of d/D values for craters located in *Zone*$_E$ and *Zone*$_{HL}$, despite the absence of ground ice in the top 0.9 km within the *Zone*$_E$, points to a $z_1/D < (z_1/D)_*$ regime in both zones. This leads to an estimate of the lower boundary of the cryosphere: $z_1 \leq$ 0.16 25 km ~ 4 km.

Finally, a patchy spatial pattern of d/D over the *Zone*$_E$ for craters in the 10 km < D < 25 km diameter range indicates spatial variability of z_0 within the *Zone*$_E$. Although many factors can cause a patchy pattern of d/D for craters in a single size bin, a progressive disintegration of the pattern over succession of bins with increasing crater size is consistent with an unevenness of z_0. In *Zone*$_E$ the minimum depth to the cryosphere has been already estimated to be $z_0^{min} \approx 0.9$ km. If the cryosphere would indeed start at $z_0 = z_0^{min}$ than all craters in the third size bin will penetrate into the cryosphere and should undergo some degree of shallowing resulting in gradual decrease of d/D everywhere in *Zone*$_E$. However, this is not what is observed. Although many *Zone*$_E$ locations on the map (the third size bin) indicate shallower craters, other another locations ("deep spots") indicate deep craters and thus $z_0 > z_0^{min}$. The deep spots on the maps corresponding to the fourth and fifth size bins are collocated with the deep spots on the map corresponding to the third size bin, but their frequencies and sizes are progressively decreasing. Thus, the base depth to ground ice in *Zone*$_E$ is $z_0^{min} \sim 0.9$ km, but deep spots, amounting to a significant fraction of the total area, exist where this depth is $z_0 \sim 1.2$ km. Within these deep spots even deeper spots exist where the depth to ground ice may be as deep as 2 km.

Conclusions: Raster maps of depth-to-diameter ratio shows spatial variability having pattern that itself changes with the size of craters. Observed patterns of crater shapes are consistent with modification of craters due to existence of cryosphere as predicted by thermodynamic models. Interpretation of spatial variability of d/D over the Terra Cimmeria region in terms of viscous relaxation alone (an simple model, used here to obtain zeroth-order estimations) yields the following numbers. The lower boundary of the cryosphere is estimated to be about 4 km. The upper boundary of the cryosphere undergoes transition at the latitude of about 40°S. Polewards of this latitude the upper boundary of the cryosphere is close to the surface. Equatorwards of this latitude the boundary is at the minimum depth of 0.9 km, but its depth appears to have spatial variability; in many places the boundary is at the depth of 1.2 km, and, in some places the boundary could be as deep as 2 km.

The CDA-based technique for mapping d/D is robust and efficient enough for the mapping to be extended to other areas on Mars, and eventually to its entire surface. Interpretation of resultant maps would lead to better understanding of distribution and character of Martian cryosphere.

References: [1] Clifford S. M. and Hillel D. (1983) *JGR, 88,* 2456-2474. [2] Fanale F. P. et al. (1986) *Icarus, 67,* 1-18. [3] Clifford S. M. (1993) *JGR, 98 E6,* 10,973-11,016. [4] Costard, F. M. (1989) *Earth, Moon, and Planets, 45,* 265-290. [5] Kuzmin, R. O. et al. (1989) *Solar System Research, 22(3),* 121-133. [6] Squyers, S. W. and Carr M. H. (1986) *Science, 231,* 249-252. [7] Jankowski, D. G. and Squyers, S. W. (1992) *Icarus 100,* 26-39. [8] Stepinski, T. F. et al. (2007) *LPS XXXVIII,* Abstract #1338. [9] Stepinski, T. F. et al. (2007) *Icarus,* submitted. [10] Smith D. et al. (2003) NASA Planetary Data System, MSG-M-MOLA-5-MEGDR-L3-V1.0. [11] Parmentier, E. M. and Head, J. W. (1981) *Icarus, 47,* 100-111. [12] Jankowski, D. G. and Squyers, S. W. (1993) *Icarus, 106,* 365-379. [13] Pathare, A. V. et al. (2005) *Icarus 174,* 396-418.